European Radiology (2021) 31:8838–8849
https://doi.org/10.1007/s00330-021-08041-2

ONCOLOGY

Comparison of contrast-enhanced CT, dual-layer detector spectral CT, and whole-body MRI in suspected metastatic breast cancer: a prospective diagnostic accuracy study

Thomas Winther Buus[1] · Finn Rasmussen[1] · Hanne Marie Nellemann[1] · Vibeke Løgager[2] · Anders Bonde Jensen[3] · Katrine Rye Hauerslev[4] · Peer Christiansen[4] · Erik Morre Pedersen[1]

Received: 9 March 2021 / Accepted: 4 May 2021 / Published online: 18 May 2021

Abstract

Objectives To compare diagnostic accuracy of contrast-enhanced CT, dual-layer detector spectral CT (DL-CT), and whole-body MRI (WB-MRI) for diagnosing metastatic breast cancer.

Methods One hundred eighty-two biopsy-verified breast cancer patients suspected of metastatic disease prospectively underwent contrast-enhanced DL-CT and WB-MRI. Two radiologists read the CT examinations with and without spectral data in consensus with 3-month washout between readings. Two other radiologists read the WB-MRI examinations in consensus. Lymph nodes, visceral lesions, and bone lesions were assessed. Readers were blinded to other test results. Reference standard was histopathology, previous or follow-up imaging, and clinical follow-up.

Results Per-lesion AUC was 0.80, 0.84, and 0.82 (CT, DL-CT, and WB-MRI, respectively). DL-CT showed significantly higher AUC than CT ($p = 0.001$) and WB-MRI ($p = 0.02$). Sensitivity and specificity of CT, DL-CT, and WB-MRI were 0.66 and 0.94, 0.75 and 0.95, and 0.65 and 0.98, respectively. DL-CT significantly improved sensitivity compared to CT ($p < 0.0001$) and WB-MRI ($p = 0.002$). Per-patient AUC was 0.85, 0.90, and 0.92 (CT, DL-CT, and WB-MRI, respectively). DL-CT and WB-MRI had significantly higher AUC than CT ($p = 0.04$ and $p = 0.03$). DL-CT significantly increased sensitivity compared to CT (0.89 vs. 0.79, $p = 0.04$). WB-MRI had significantly higher specificity than CT (0.84 vs. 0.96, $p = 0.001$) and DL-CT (0.87 vs. 0.96, $p = 0.02$).

Conclusions DL-CT showed significantly higher per-lesion diagnostic performance and sensitivity than CT and WB-MRI. On a per-patient basis, DL-CT and WB-MRI had equal diagnostic performance superior to CT.

Key Points

- *Spectral CT has higher diagnostic performance for diagnosing breast cancer metastases compared to conventional CT and whole-body MRI on a per-lesion basis.*
- *Spectral CT and whole-body MRI are superior to conventional CT for diagnosing patients with metastatic breast cancer.*
- *Whole-body MRI is superior to conventional CT and spectral CT for diagnosing bone metastases.*

Keywords Breast neoplasms · Neoplasm staging · Whole-body imaging · Tomography, X-ray computed · Diffusion magnetic resonance imaging

✉ Thomas Winther Buus
thomas.winther.buus@auh.rm.dk

[1] Department of Radiology, Aarhus University Hospital, Palle Juul-Jensens Boulevard 99, 8200 Aarhus N, Denmark

[2] Department of Radiology, Herlev Hospital, Borgmester Ib Juuls Vej 17, 2730 Herlev, Denmark

[3] Department of Oncology, Aarhus University Hospital, Palle Juul-Jensens Boulevard 99, 8200 Aarhus N, Denmark

[4] Department of Plastic and Breast Surgery, Aarhus University Hospital, Palle Juul-Jensens Boulevard 35, 8200 Aarhus N, Denmark

Abbreviations

ADC	Apparent diffusion coefficient
AUC	Area under the curve
DE-CT	Dual-energy computed tomography
DL-CT	Dual-layer detector spectral computed tomography
DWI	Diffusion-weighted imaging
DWIBS	Diffusion-weighted whole-body imaging with background body signal suppression

PET/CT	Positron emission tomography/computed tomography
ROC	Receiver operating characteristics
WB-MRI	Whole-body magnetic resonance imaging

Introduction

Breast cancer is the most frequent cancer affecting women and the second leading cause of cancer-related deaths [1]. The 5-year survival rate is deeply related to the presence of metastases; dropping from around 85% in patients undergoing curative intended treatment to < 25% in patients with metastatic disease [2]. International clinical practice guidelines do not recommend whole-body imaging in asymptomatic patients with early-stage disease [3, 4]. In patients with symptoms of metastatic disease or advanced locoregional disease, a diagnostic workup is indicated, but no consensus exists as to which modality should be used [5]. Often, CT and bone scintigraphy are used, although their sensitivity and specificity for detecting lytic bone metastases are low [6–9].

Whole-body magnetic resonance imaging (WB-MRI) has sensitivity and specificity in detecting breast cancer bone metastases comparable to positron emission tomography/computed tomography (PET/CT) [9, 10]. The introduction of whole-body diffusion-weighted imaging (DWI) with background body signal suppression (DWIBS) [11] improved the ability to detect malignancies through increased tissue contrast and the use of apparent diffusion coefficient (ADC) values [12]. In addition to lesion detection, WB-MRI has been shown to be superior to CT for treatment response assessment of metastatic breast cancer [13] and a standard for WB-MRI protocols has been proposed [14].

Dual-energy computed tomography (DE-CT) is an emerging CT technique that provides quantitative measures of material concentrations and decompositions as well as the ability to suppress or enhance materials such as iodine, water, calcium, or uric acid [15, 16]. Different technical approaches can generate a difference in attenuation between two different photon energies, such as dual-layer detector spectral CT (DL-CT) [17], where the top detector layer detects low-energy photons and the bottom detector layer detects high-energy photons [16, 18, 19]. This removes the previous need for changing scan parameters. The improvement in iodine visualisation and quantitation offered by DE-CT, as well as the ability to suppress materials, has been shown to increase the sensitivity for diagnosing a range of primary tumours [19] as well as bone metastases [20]. In addition, DL-CT has been shown to increase the confidence of radiologists and reduce the need for additional examinations in patients suspected of malignancy [21].

However, studies investigating the diagnostic accuracy of WB-MRI in metastatic breast cancer have mainly focused on bone metastases [22] or assessed visceral metastases in small studies [23] while the diagnostic accuracy of DL-CT remains to be investigated completely. Because of the importance of diagnostic imaging for treatment guidance and the lack of consensus as to which modality should be used, prospective studies comparing WB-MRI and DL-CT with conventional imaging techniques for metastasis detection are needed.

The aim of our study was to assess and compare the diagnostic accuracy of CT, DL-CT, and WB-MRI in women with suspected metastatic breast cancer.

Materials and methods

Patients

Patients were prospectively enrolled at the Department of Oncology and Department of Plastic and Breast Surgery. The inclusion criteria were as follows: women, age ≥ 18 years, present or prior biopsy-verified breast cancer, referred for diagnostic workup on a suspicion of metastatic disease. The most common indications for referral were bone pain, weight loss, decreasing general condition, recurrent ipsilateral breast cancer, suspicious imaging findings, and advanced locoregional disease. Exclusion criteria were as follows: previous hypersensitivity reactions to both iodixanol and iohexol or anaphylactic reactions to any iodinated contrast agent, pregnancy, renal insufficiency (estimated glomerular filtration rate < 30 mL/min), claustrophobia, or foreign bodies contraindicating MRI (breast implants were not a contraindication [24]).

Dual-layer detector spectral CT protocol

All DL-CT examinations were acquired on a 64-row dual-layer detector spectral CT scanner (IQon, Philips Healthcare) using the following acquisition parameters: kV peak, 120–140; mA/s, 150–250; rotation time, 0.75 s; pitch, 1.078; collimation, 64 × 0.625 mm; matrix, 512 × 512; acquired slice thickness, 0.625 mm; reconstructed slice thickness, 2 mm; increment, 1 mm. Iodixanol 320 mg/mL (Visipaque 320, GE Healthcare) was administered intravenously in weight-adjusted doses of 2 mL/kg using a pre-set injection rate of 4 mL/s. If the patient previously had minor adverse effects on iodixanol (such as nausea, vomiting, or mild urticaria), iohexol 350 mg/mL (Omnipaque 350, GE Healthcare) was used instead. Bolus tracking was used to time the scan phase with a region of interest placed in the descending thoracic aorta using a threshold of 150 HU. Contrast-enhanced DL-CT of the chest and upper abdomen was acquired in the arterial phase (15 s delay post threshold) while DL-CT of the abdomen and pelvis was acquired in the portal venous phase (65s delay post threshold). Conventional CT images were reconstructed from weighted addition of the two detector layers' signals. The conventional CT images did not differ from single-energy CT in dose [25] or image quality [26]. In

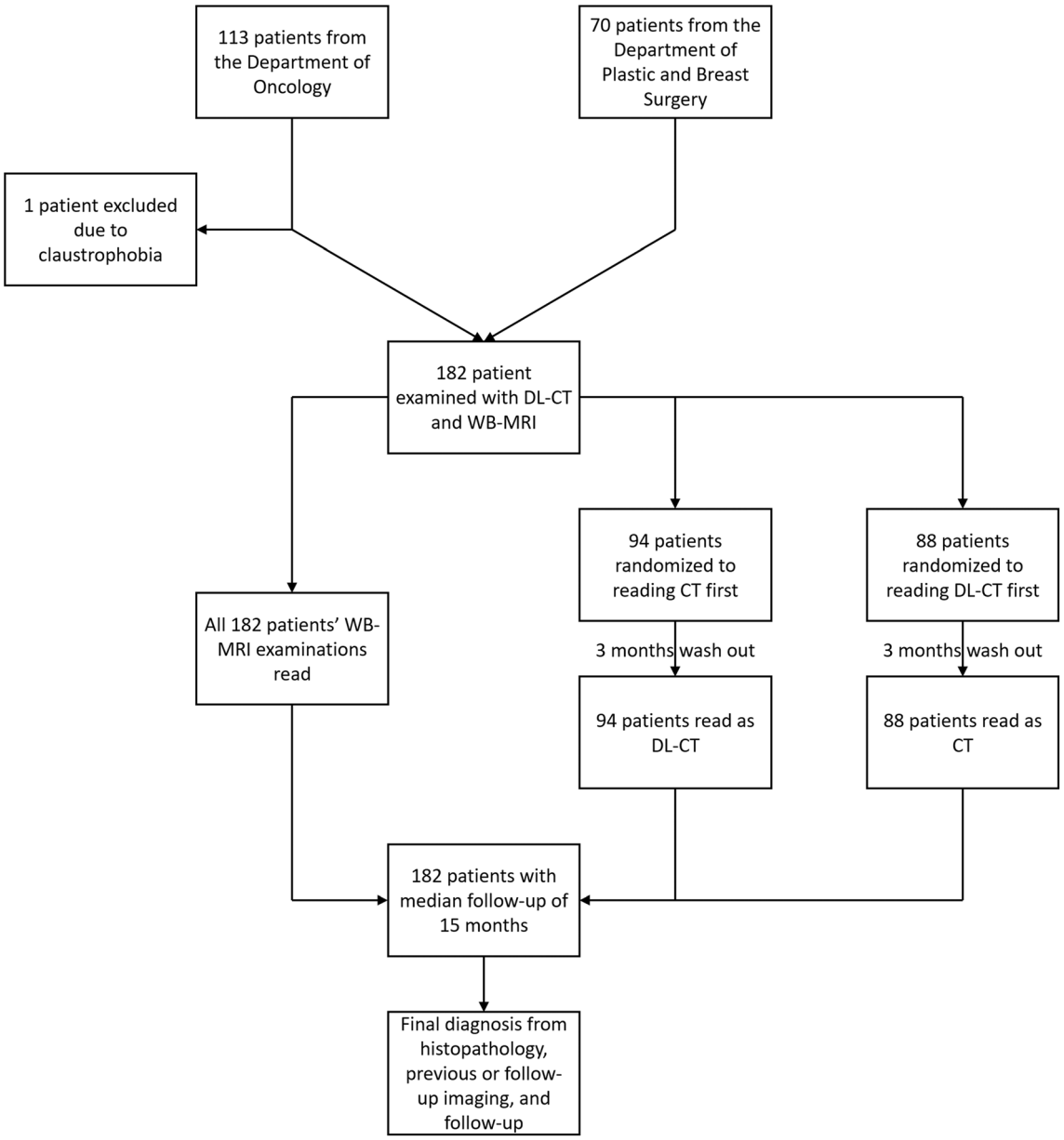

Fig. 1 Flowchart showing patient enrolment and the reading set-up. DL-CT = dual-layer detector spectral CT, WB-MRI = whole-body MRI

addition, spectral base images were reconstructed by spectral separation of the two detector layers' signals.

Whole-body MRI protocol

All MRI examinations were acquired using a 1.5T MRI system (Ingenia, Philips Healthcare) with built-in posterior coil, head and neck coil, and flex coverage anterior coil from the scanner vendor. The MRI protocol consisted of sagittal T1-weighted and sagittal T2-weighted Dixon images of the spine, axial DWI (b = 0, 50, and 800), axial T1-weighted Dixon, axial T2-weighted, and coronal T1-weighted images from the skull base to mid-thighs, and axial DWI (b = 200) of the lungs (Supplementary Table 1). DWI was acquired with short-tau inversion recovery fat suppression using an inversion time of 180 ms. Mono-exponential ADC maps were calculated using the b50 and b800 images. From axial T1-weighted Dixon images and sagittal T2-weighted Dixon images, fat fraction images were calculated as fat/in-phase. The scan time was 25:32.

Image interpretation

All imaging data were anonymised and randomised, and readers only had access to patient age. Conventional CT and DL-CT datasets were transferred to a spectral workstation for analysis (IntelliSpace Portal 9.0, Philips Healthcare). Available

Table 1 Diagnostic criteria used for detecting metastases with the three imaging modalities. DL-CT = dual-layer detector spectral CT; WB-MRI = whole-body MRI; ADC = apparent diffusion coefficient. *See Supplementary Table 2

Metastatic criteria	CT	DL-CT	WB-MRI
Lymph nodes	Short axis ≥ 10 mm	Short axis ≥ 10 mm OR Short axis < 10 mm with loss of fatty hilum and iodine density > 0.5 mg/ml	Short axis ≥ 10 mm OR Short axis < 10 mm with loss of fatty hilum and increased signal intensity on b800 images compared to benign-appearing lymph nodes
Lung metastases	Solitary nodule > 8 mm OR Multiple nodules ≤ 8 mm	Solitary nodule > 8 mm OR Solitary nodule ≤ 8 mm with clear iodine attenuation or affecting surrounding lung tissue on Z effective images OR Multiple nodules ≤ 8 mm	Solitary nodule > 8 mm on b200 images OR Multiple nodules ≤ 8 mm on b200 images
Liver metastases	Suspicious lesion > 20 HU	Suspicious lesion > 20 HU AND Non-yellow appearance on Z effective images	High signal intensity on b800 images and ADC values < 1.5×10^{-3} mm^2/s AND Appearance on T2-weighted images not consistent with cysts
Bone metastases	Suspicious lytic or sclerotic lesion	Suspicious lytic or sclerotic lesion	High signal intensity on b800 images with ADC values higher than surrounding bone AND Low-signal intensity on T1-weighted and T2-weighted Dixon fat fraction images
Ovarian tumours/metastases	Solid tumour OR Cystic lesion with septae and/or nodules with contrast enhancement OR Cystic lesion > 5 cm in patient > 50 years	Solid tumour OR Cystic lesion with septae and/or nodules with contrast enhan cement OR Cystic lesion > 5 cm in patient > 50 years	Solid tumour with high signal intensity on b800 images and ADC values < 1.5×10^{-3} mm^2/s OR Cystic lesion with septae and/or nodules with diffusion restriction OR Cystic lesion > 5 cm in patient > 50 years
Kidney tumours	Solid tumour OR ≥ Bosniak IIF	Solid tumour OR ≥ Bosniak IIF	Solid tumour OR ≥ Bosniak IIF
Other tumours/metastases*	Suspicious lesion	Suspicious lesion with non-yellow appearance on Z effective images with clear iodine attenuation	Suspicious lesion with high signal intensity on b800 images and ADC values < 1.5×10^{-3} mm^2/s

spectral data included the following: virtual mono-energetic images (40–200 keV), effective atomic number (Z effective; shows the atomic number of the tissue), iodine density images (shows the iodine concentration in mg/mL), virtual non-contrast images (70 keV images without the attenuation from iodine). Overlay of any spectral parameter onto conventional series was available. The CT and DL-CT examinations were read in consensus by two radiologists with 35 and 30 years of radiological experience, respectively. The reading of the CT and DL-CT examinations was divided into two readings separated by a 3-month washout period to reduce recall bias (Fig. 1). Reading time of both CT and DL-CT were recorded.

All 182 WB-MRI examinations were analysed using Osirix version 10 (Pixmeo) in consensus by two radiologists with 18 and 12 years of experience in body MRI, respectively. In addition to the acquired MRI sequences, a colour-coded overlay of b800 images onto T2-weighted images was available on the workstation [27].

A RedCAP database [28] was used to register all imaging findings. Up to three lesions per region were recorded each for lungs, liver, and bones, and up to 5 lesions for "other". The category "other" included pleural metastases, peritoneal carcinomatosis, ovarian metastases, and possible malignant lesions not associated with breast cancer (Supplementary Table 2). In addition, up to three pathological appearing lymph nodes in any region were recorded. The criteria used for diagnosing metastases are shown in Table 1. Confidence

Table 2 Patient demographics. HER2 = human epidermal growth factor receptor 2; SLNB = sentinel lymph node biopsy; ALND = axillary lymph node dissection

Patient demographics	Department of Oncology	Department of Plastic and Breast Surgery
Number of patients	112	70
Age (years)	59.3 ± 12.3	62.0 ± 15.8
Indications for referral		
Bone pain	49 (44%)	0 (0%)
Recurrent breast cancer	0 (0%)	34 (49%)
Locally advanced breast cancer	12 (11%)	20 (29%)
Suspicious findings on other imaging	11 (10%)	11 (16%)
Suspicious biochemistry	19 (17%)	0 (0%)
Miscellaneous reasons	21 (19%)	5 (7%)
Side of primary tumour		
Right	69 (62%)	35 (50%)
Left	41 (37%)	27 (39%)
Bilateral	2 (2%)	8 (11%)
Previous breast surgery		
Breast-conserving	49 (44%)	20 (29%)
Mastectomy	56 (50%)	29 (41%)
None	7 (6%)	21 (30%)
Type of primary tumour		
Invasive ductal carcinoma	83 (74%)	56 (80%)
Invasive lobular carcinoma	13 (12%)	7 (10%)
Ductal carcinoma in situ	5 (4%)	2 (3%)
Other	11 (10%)	5 (7%)
Estrogen receptor–positive		
Yes	97 (87%)	57 (81%)
No	15 (13%)	13 (19%)
HER2-positive		
Yes	19 (17%)	8 (11%)
No	93 (83%)	62 (89%)
Grade		
I	14 (13%)	7 (10%)
II	44 (39%)	37 (53%)
III	29 (26%)	11 (16%)
Missing	25 (22%)	15 (21%)
Previous SLNB		
Yes	108 (96%)	42 (60%)
No	4 (4%)	28 (40%)
Previous ALND		
Yes	56 (50%)	17 (24%)
No	56 (50%)	53 (76%)
Adjuvant chemotherapy and/or radiotherapy		
Yes	100 (89%)	28 (40%)
No	12 (11%)	42 (60%)
Years since first diagnosis, median (range)	2 (0–24)	0.5 (0–29)
Size of primary tumour (mm)	24.7 ± 21.7	25.6 ± 21.1

of malignancy for each lesion was scored as 1, benign; 2, probably benign; 3, indeterminate; 4, probably malignant; and 5, malignant. Scores of 1–3 were considered benign, whereas 4–5 were considered malignant. Overlooked lesions or lesions not mentioned during the reading were assigned a score of 1. Each region was assigned the highest lesion score in that region for the per region analysis. For the per-patient analysis, true positive was defined as at least one correctly diagnosed metastasis, while true negative was defined as all lesions correctly diagnosed as benign.

Reference standard

All patients were being followed at the Department of Oncology with a clinical examination and blood tests for 5 years after definitive surgery. After a median of 18-month follow-up (range: 13–34) after completing the WB-MRI and DL-CT examinations, the clinical status of each patient was assessed. Medical records including histopathology reports, prior imaging, and follow-up imaging were used to classify each lesion. Histopathology was considered the gold standard where available. Lesions without histopathologic verification were considered malignant if they showed progression (or regression/disappeared if the patient were under treatment) on follow-up imaging. In case of no changes on follow-up imaging through at least 12 months, the lesion was considered benign. Lesions appearing on follow-up imaging, which could not be seen on WB-MRI or DL-CT, were considered overlooked lesions. Lesions which could neither be verified by histopathology or follow-up imaging were considered malignant if the lesion was absent on previous imaging performed within the last 5 years. If the lesion was present on previous imaging and appeared unchanged through at least 2 years, it was considered benign. In patients with no biopsies performed and no previous or follow-up imaging, any lesion was considered benign after a median clinical follow-up of 22 months (range: 13–34).

Statistical analysis

STATA Statistics/Data analysis Special Edition version 16.1 (StataCorp) was used for all statistical analyses.

This study was powered to show a 10% difference in sensitivity on a per-lesion basis using a significance level of 0.05 and power of 0.80. Assuming a prevalence of metastatic disease of 30% and an average of 3 metastatic lesions per positive patient, the sample size was calculated to 182 patients. Receiver operating characteristics (ROC) curves were constructed based on the 5-point assessments from the reviewers on a per-lesion basis and on a per-patient basis. From the ROC curves,

Table 3 Reference standard used for verification of each lesion. The number of suspicious axillary lymph nodes on whole-body MRI and dual-layer detector spectral CT was matched with the number of metastatic axillary lymph nodes from the histopathology reports obtained from sentinel lymph node biopsy or axillary dissection. US = ultrasonography; ^{18}F-FDG PET/CT = ^{18}F-fluorodeoxyglucose positron emission tomography/computed tomography

Reference standard	All lesions		Lymph nodes		Lung		Liver		Bone		Other	
	Metastatic	Benign	Metastatic	Benign	Metastatic	Benign	Metastatic	Benign	Metastatic	Benign	Metastatic	Benign
Follow-up		198				18		41		58		81
Histopathology	155	24	83	9	4	3	20		31	3	17	9
Follow-up imaging												
CT	80	214	26	8	18	32	11	60	16	12	9	102
MRI	44	9							44	9		
US		22						12				10
^{18}F-FDG PET/CT	10	35	5		3	8		7		4	2	16
Previous imaging												
CT	28	162	14	6	9	18		59	2	5	3	74
MRI	3	3							3	3		
US		16						5				11
Scintigraphy		2										2
^{18}F-FDG PET/CT		4										4

the area under the curve (AUC) was calculated and used for comparison of the diagnostic performance of the three imaging modalities using the DeLong approach [29]. Comparison of sensitivity and specificity was done using McNemar [30]. Differences in reading times of CT and DL-CT were compared using a one-sample *t*-test. A p value < 0.05 was considered statistically significant without adjustment for multiple testing.

Results

Patients

From April 2018 to November 2019, 183 patients were consecutively enrolled. Of 183 patients enrolled, one patient was excluded due to claustrophobia. Patient demographics are shown in Table 2. Median time from referral to imaging was

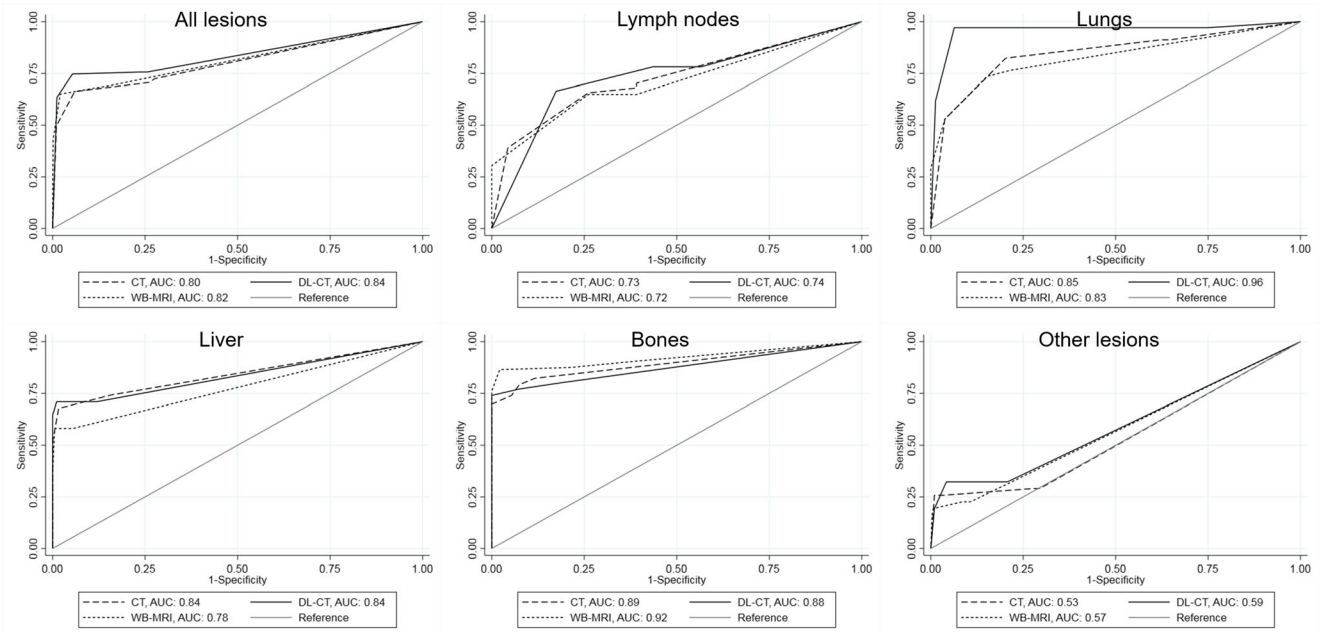

Fig. 2 Receiver operating characteristics curves for conventional CT, dual-layer detector spectral CT (DL-CT), and whole-body MRI (WB-MRI) on a per-lesion basis. AUC = area under the curve

Table 4 Diagnostic performance of CT, dual-layer detector spectral CT (DL-CT), and whole-body MRI (WB-MRI) on a per-lesion basis. † denotes significantly better performance than CT; ‡ denotes significantly better performance than DL-CT; and * denotes significantly better performance than WB-MRI. AUC = area under the curve

	Number of lesions	Metastatic lesions	Benign lesions	AUC	Sensitivity	Specificity	Correctly classified
All lesions	1009	320	689				
CT		212	648	0.80	0.66	0.94	0.85
DL-CT		239	652	0.84†*	0.75†*	0.95	0.88
WB-MRI		208	675	0.82	0.65	0.98†	0.88
Lymph nodes	151	128	23				
CT		84	17	0.73	0.66	0.74	0.69
DL-CT		100	13	0.74	0.78†*	0.57	0.57
WB-MRI		83	17	0.72	0.65	0.74	0.66
Lung lesions	113	34	79				
CT		28	63	0.85	0.82*	0.80	0.81
DL-CT		33	74	0.96†*	0.97†*	0.94†	0.95
WB-MRI		18	76	0.83	0.53	0.96†	0.83
Liver lesions	215	31	184				
CT		21	181	0.84	0.68	0.98	0.94
DL-CT		22	182	0.84*	0.71	0.99	0.95
WB-MRI		18	183	0.78	0.58	0.99	0.93
Bone lesions	190	96	94				
CT		71	89	0.89	0.74	0.95	0.84
DL-CT		74	87	0.88	0.77	0.93	0.85
WB-MRI		83	92	0.92†‡	0.86†	0.98	0.92
Other lesions	340	31	309				
CT		8	298	0.53	0.26	0.96	0.90
DL-CT		10	296	0.59	0.32	0.96	0.90
WB-MRI		6	307	0.57	0.19	0.99†‡	0.92

4 days (range 1–13, with one patient being examined 26 days after referral due to her wishing to go on vacation).

A total of 66 patients (36%) were diagnosed with metastatic disease. Of these 66 patients, 38 patients (58%) had metastases in one region, 9 patients (14%) in two regions, 7 patients (11%) in three regions, and 12 patients (18%) in four regions. All of the 66 patients had at least one metastatic lesion verified by biopsy.

A total of 1009 lesions (320 metastatic and 689 benign lesions) were assessed. Table 3 shows lesions by anatomical region and reference used for diagnosis. The size of the benign lesions was 13.3 ± 11.9 mm vs 15.1 ± 15.1 mm for the metastatic lesions ($p = 0.23$) (short axis for lymph nodes and long axis for non-lymph node lesions).

Per-lesion analysis

The reading time of DL-CT was significantly longer than that of CT (308 s vs 256 s, $p = 0.02$).

DL-CT had the highest diagnostic performance of the three imaging modalities on a per-lesion basis as illustrated by the ROC curves in Fig. 2. DL-CT had significantly higher AUC compared to both CT and WB-MRI for all lesions ($p = 0.001$ and $p = 0.02$, respectively) and lung lesions ($p = 0.002$ and $p < 0.0001$, respectively), and also had higher AUC than WB-MRI for liver lesions ($p < 0.05$). WB-MRI had significantly higher AUC compared to both CT and DL-CT for bone lesions ($p = 0.003$ and $p = 0.007$, respectively).

Sensitivity and specificity for the three imaging modalities on a per-lesion basis are shown in Table 4. The sensitivity of CT, DL-CT, and WB-MRI for all lesions was 0.66, 0.75, and 0.65, respectively. DL-CT showed significantly higher sensitivity compared to both CT and WB-MRI for all lesions ($p < 0.0001$ and $p = 0.002$, respectively), lymph node metastases ($p = 0.009$ and $p < 0.0001$), and lung metastases ($p = 0.002$ and $p < 0.0001$), while CT showed significantly higher sensitivity than WB-MRI for lung metastases ($p = 0.02$). WB-MRI had significantly higher sensitivity than CT ($p = 0.01$) but not DL-CT ($p = 0.06$) for detecting bone metastases. The specificity of CT, DL-CT, and WB-MRI for all lesions was 0.94, 0.95, and 0.98, respectively. DL-CT and WB-MRI had significantly higher specificity compared to CT for lung lesions ($p = 0.0002$ and $p = 0.02$). WB-MRI had significantly higher specificity than CT and DL-CT for other

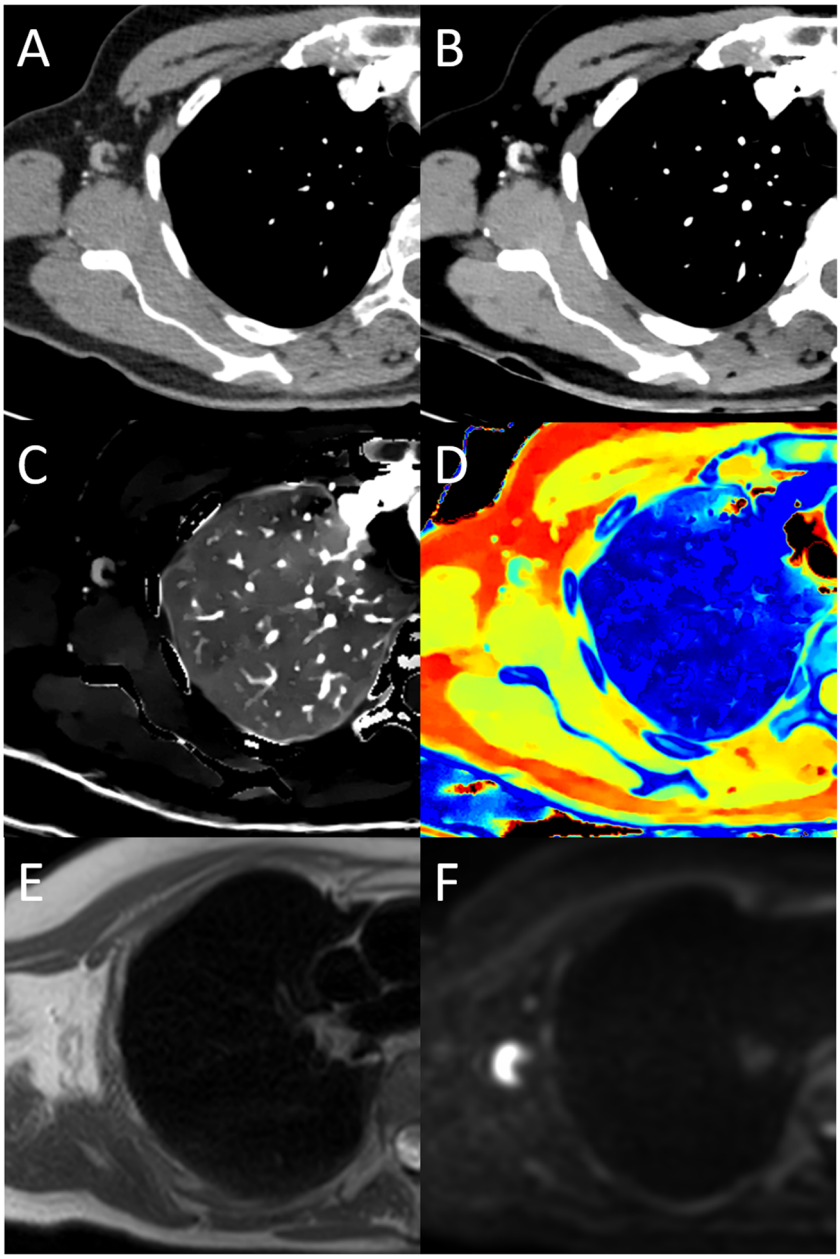

Fig. 3 Patient with a metastatic lymph node in the right axilla. The lymph node appears morphologically benign on conventional CT (**A**) with preserved fatty hilum and a short axis < 5 mm. On mono-energetic images (40 keV) (**B**), the lymph node shows clear contrast enhancement, and the iodine concentration is measured to > 2 mg/ml on iodine density images (**C**). The lymph node is coloured green on Z effective images (**D**) further suggesting increased iodine enhancement. The lymph node appears benign on T2-weighted images with a short axis < 10 mm and no loss of the fatty hilum (**E**), although it has high signal intensity on b800 images (**F**). The apparent diffusion coefficient value was measured to 1.2×10^{-3} mm/s. The lymph node was diagnosed as metastatic by biopsy

lesions ($p = 0.02$ and $p = 0.007$) and significantly higher specificity for all lesions than CT ($p = 0.0001$).

Figures 3 and 4 show examples of a metastatic lymph node and lung nodules correctly diagnosed only by DL-CT. Figure 5 shows an example with a bone metastasis correctly diagnosed on WB-MRI not visible on either CT or DL-CT.

Per-patient analysis

Both DL-CT and WB-MRI had significantly higher AUC compared to CT on a per-patient basis ($p = 0.04$ and $p = 0.03$) as shown by the ROC curves in Fig. 6. Table 5 shows AUC, sensitivity, and specificity on a per-patient basis for the three imaging modalities.

Sensitivity of CT, DL-CT, and WB-MRI on a per-patient basis was 0.79, 0.89, and 0.82, respectively. DL-CT significantly increased sensitivity compared to CT ($p = 0.04$).

The specificity of CT, DL-CT, and WB-MRI on a per-patient basis was 0.84, 0.87, and 0.96, respectively. WB-MRI had significantly higher specificity compared to both CT and DL-CT ($p = 0.001$ and $p = 0.02$) on a per-patient basis.

Discussion

In the present study, the diagnostic performance of DL-CT and WB-MRI were significantly higher than conventional CT for diagnosing metastatic breast cancer on a per-patient

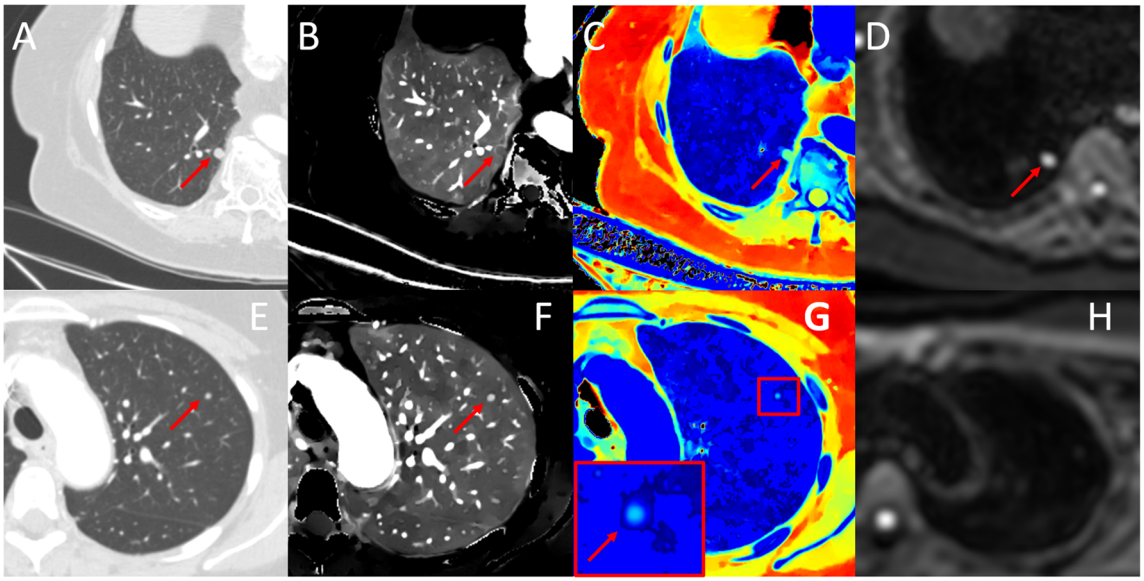

Fig. 4 **A**–**D** Patient with a benign lung nodule in the right lower lobe (red arrows). The nodule was considered metastatic by conventional CT (**A**) and whole-body MRI (WB-MRI) (**D** shows an image from the b200 lung sequence). However, the nodule has low iodine concentration (< 0.5 mg/ml) on iodine density images (**B**) and appears to be attached to the pleura on Z effective images (**C**). The nodule was considered benign on dual-layer detector CT (DL-CT) and was diagnosed as benign on follow-up ^{18}F-FDG PET/CT. **E**–**H** Another patient with lung metastasis in the left upper lobe (red arrows). The lesion was too small to be characterised on conventional CT (**E**) and is not visible on the b200 lung sequence (**H**). On iodine density images (**F**), the iodine concentration in the nodule was measured to > 3 mg/ml. Z effective images show an area of lung tissue surrounding the lesion (**G**) affected by the lesion (red arrow in the magnified image). The nodule was considered metastatic on DL-CT and was diagnosed as metastatic by showing clear progression in size on follow-up CT

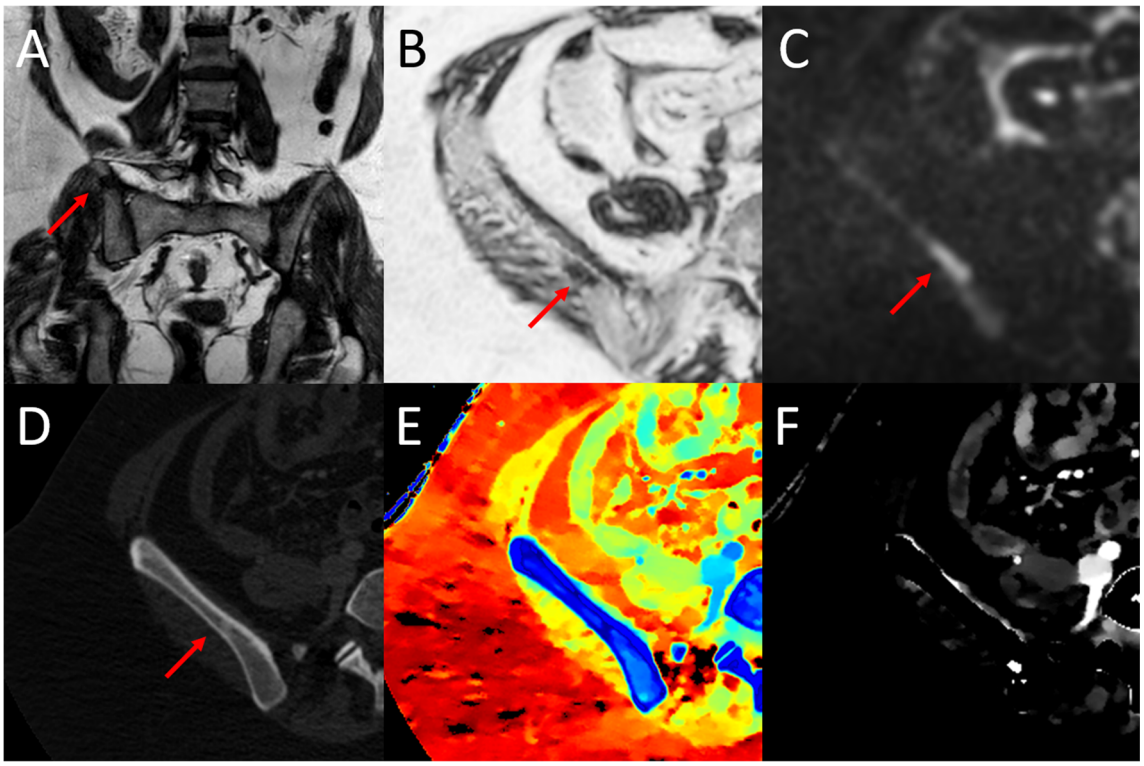

Fig. 5 Patient with a metastasis in the right iliac bone. The lesion (red arrows) is visible as a dark area on coronal T1-weighted images (**A**) and axial fat fraction images (**B**) derived from the T1-weighted Dixon images. On b800 images (**C**), the lesion shows clear diffusion restriction compared to the surrounding bone. The lesion is barely visible on conventional CT images (**D**) and was overlooked by the CT readers in both readings. Z effective images (**E**) and iodine density images (**F**) did not increase lesion conspicuity. The lesion was confirmed as metastatic by CT-guided biopsy

Table 5 Diagnostic performance of CT, dual-layer detector spectral CT (DL-CT), and whole-body MRI (WB-MRI) on a per-patient basis. † denotes significantly better performance than CT and ‡ denotes significantly better performance than DL-CT. AUC = area under the curve

	Assessed	With metastases	No metastases	AUC	Sensitivity	Specificity	Correctly classified
Patients	182	66	116				
CT		52	98	0.85	0.79	0.84	0.82
DL-CT		59	101	0.90†	0.89†	0.87	0.88
WB-MRI		54	111	0.92†	0.82	0.96†‡	0.91
Lymph nodes	182	48	134				
CT		35	130	0.88	0.73	0.97	0.91
DL-CT		41	129	0.92	0.85	0.96	0.93
WB-MRI		37	132	0.88	0.77	0.99	0.93
Lungs	182	13	169				
CT		11	158	0.96	0.85	0.93	0.93
DL-CT		12	165	0.95	0.92	0.98	0.97
WB-MRI		7	166	0.90	0.54	0.98	0.95
Liver	182	11	171				
CT		8	170	0.89	0.73	0.99	0.98
DL-CT		8	170	0.85	0.73	0.99	0.98
WB-MRI		7	170	0.81	0.64	0.99	0.97
Bones	182	35	147				
CT		26	144	0.91	0.74	0.98	0.93
DL-CT		27	144	0.89	0.77	0.98	0.94
WB-MRI		31	146	0.95	0.89	0.99	0.97
Other	182	14	168				
CT		7	157	0.65	0.50	0.93	0.90
DL-CT		10	158	0.75	0.71	0.94	0.92
WB-MRI		6	166	0.65	0.43	0.99	0.95

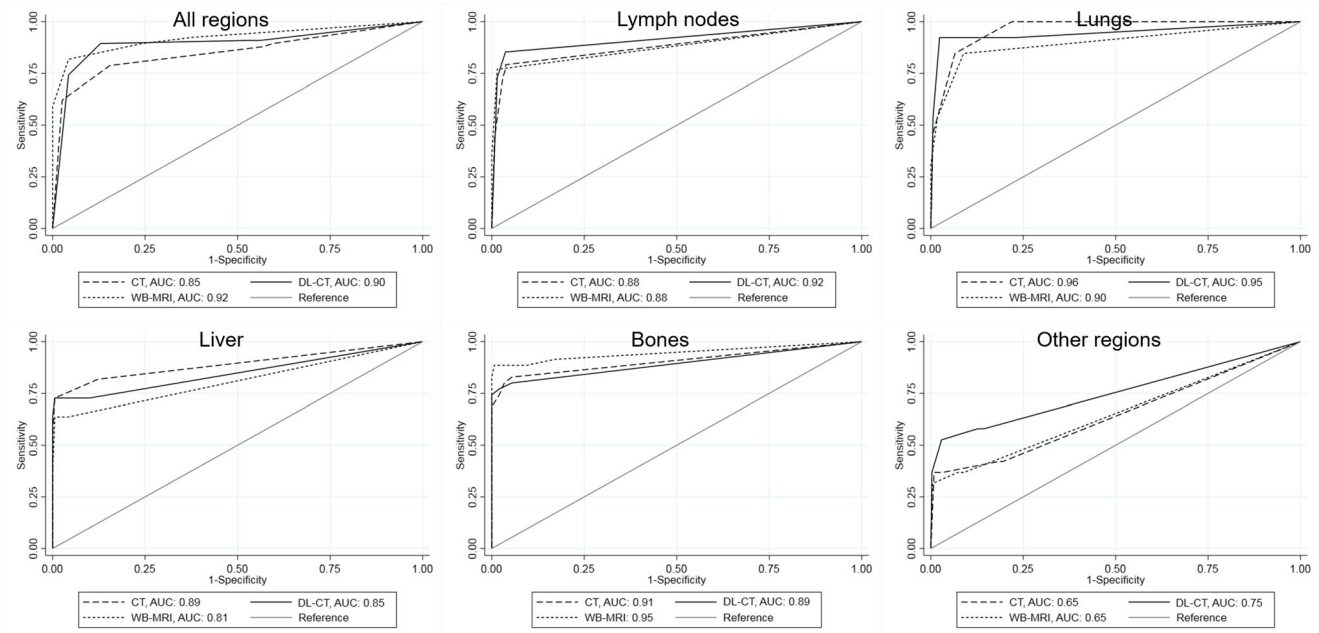

Fig. 6 Receiver operating characteristics curves for conventional CT, dual-layer detector spectral CT (DL-CT), and whole-body MRI (WB-MRI) on a per-patient basis. AUC = area under the curve

basis. DL-CT had significantly higher sensitivity compared to CT while WB-MRI had superior specificity. On a per-lesion basis, DL-CT showed significantly higher diagnostic performance and sensitivity than both CT and WB-MRI. This is in agreement with a previous study by Andersen et al [21] which showed increased sensitivity for DL-CT compared to CT in patients suspected of malignancy. As was the case in the study by Andersen et al [21], we found increased reading time of DL-CT compared to CT, although the increase was minor (< one minute) considering the benefit of the increased diagnostic performance of DL-CT.

DL-CT had significantly higher sensitivity for detecting lymph node metastases compared to CT and WB-MRI, although the specificity was lower. The increased sensitivity of DL-CT was achieved by using an iodine concentration of 0.5 mg/mL as cut-off between metastatic and non-metastatic lymph nodes in morphologically suspicious nodes. Metastatic axillary lymph nodes have previously been shown to have significantly higher iodine density compared to non-metastatic lymph nodes [31]. However, the cut-off of 0.5 mg/mL iodine in our study was likely too low given the low specificity of DL-CT for diagnosing lymph node metastases. In a study by Volterrani et al [32], they showed an optimal cut-off value of 1.7 mg/mL iodine for differentiating malignant breast lesions from benign breast lesions. Applying a higher cut-off may increase the diagnostic performance of DL-CT for diagnosing lymph node metastases.

In the lungs, DL-CT increased sensitivity compared to CT and WB-MRI and specificity compared to CT. The use of iodine density images to assess contrast enhancement of small lung nodules and Z effective images to visualise peri-lesion involvement allowed several lung lesions to be correctly diagnosed by DL-CT. In a study by Chao et al [33], malignant lung nodules showed increased contrast enhancement on DE-CT. In another study [34], iodine density was correlated with SUVmax (a marker of tumour glucose metabolism) in malignant lung nodules. Z effective and iodine density images may be of value in discriminating malignant and benign lung nodules.

WB-MRI had significantly higher diagnostic performance than CT and DL-CT for diagnosing bone lesions. In a study by Abdullayev et al [20], they used multi-level virtual non-calcium reconstructions of DL-CT examinations to suppress calcium in the bones. With calcium suppressed, they were able to show increased sensitivity and specificity in detecting vertebral bone metastases. Unfortunately, calcium suppression was not commercially available at the time of our study. Since bone lesions were the only region where DL-CT was inferior to WB-MRI, the implementation of calcium suppression could potentially be important for establishing DL-CT as a stand-alone modality for the diagnostic workup of metastatic breast cancer.

The main strengths of our study were the prospective study design and the large patient cohort. The patients had DL-CT and WB-MRI examinations performed on the same day, and the assessments were made by experienced readers blinded to the results of the other imaging modalities.

Our study had some limitations. First, we only had pathological verification for 155/320 metastatic lesions and 24/689 benign lesions and had to rely on previous and follow-up imaging. In addition, for 198/689 benign lesions, no previous or follow-up imaging was available. However, all patients with metastatic disease had at least one biopsy-verified lesion. Second, we did not assess inter-reader reliability as the examinations were read in consensus. Finally, our study was conducted at a single centre which restricts the generalisation of the results.

In conclusion, DL-CT and WB-MRI appear equal in diagnostic performance on a per-patient basis and are preferable to conventional CT. On a per-lesion basis, DL-CT had significantly higher diagnostic performance compared to both CT and WB-MRI, although slightly lower than WB-MRI in the bones. Future prospective multi-centre studies comparing DL-CT and WB-MRI with functional imaging techniques, such as PET/CT, are needed to determine the optimal choice of imaging in breast cancer patients suspected of metastatic disease.

Supplementary Information The online version contains supplementary material available at https://doi.org/10.1007/s00330-021-08041-2.

Acknowledgements The authors would like to thank research radiographer Olga Vendelbo for helping set up scan protocols and scanning the patients.

Funding This study was supported by the Health Research Foundation of Central Denmark Region.

Declarations

Guarantor Erik Morre Pedersen, MD PhD DMSc.

Conflict of Interest The authors of this manuscript declare no relationships with any companies whose products or services may be related to the subject matter of the article.

Statistics and Biometry No complex statistical methods were necessary for this paper.

Informed Consent Prior to DL-CT and WB-MRI, written informed consent was obtained from all subjects (patients) in this study.

Ethical Approval Institutional Review Board approval was obtained. This prospective single-centre study was approved by the Central Denmark Region Committee on Health Research Ethics (reference number 1-10-72-425-17) and was conducted between April 2018 and November 2019.

Methodology
- prospective
- diagnostic study
- performed at one institution

References

1. Bray F, Ferlay J, Soerjomataram I et al (2018) Global cancer statistics 2018: GLOBOCAN estimates of incidence and mortality worldwide for 36 cancers in 185 countries. CA Cancer J Clin 68: 394–424
2. Siegel RL, Miller KD, Jemal A (2018) Cancer statistics, 2018. CA Cancer J Clin 68:7–30
3. Cardoso F, Kyriakides S, Ohno S et al (2019) Early breast cancer: ESMO Clinical Practice Guidelines for diagnosis, treatment and follow-up. Ann Oncol 30:1194–1220
4. Khatcheressian JL, Hurley P, Bantug E et al (2013) Breast cancer follow-up and management after primary treatment: American society of clinical oncology clinical practice guideline update. J Clin Oncol 31:961–965
5. Cardoso F, Senkus E, Costa A et al (2018) 4th ESO-ESMO international consensus guidelines for advanced breast cancer (ABC 4). Ann Oncol 29:1634–1657
6. Haraldsen A, Bluhme H, Røhl L et al (2016) Single photon emission computed tomography (SPECT) and SPECT/low-dose computerized tomography did not increase sensitivity or specificity compared to planar bone scintigraphy for detection of bone metastases in advanced breast cancer. Clin Physiol Funct Imaging 36:40–46
7. Hamaoka T, Madewell JE, Podoloff D a et al (2004) Bone imaging in metastatic breast cancer. J Clin Oncol 22:2942–2953
8. Hildebrandt MG, Gerke O, Baun C et al (2016) [181F] Fluorodeoxyglucose (FDG)-positron emission tomography (PET)/computed tomography (CT) in suspected recurrent breast cancer: a prospective comparative study of dual-time-point FDG-PET/CT, contrast-enhanced CT, and bone scintigraphy. J Clin Oncol 34:1889–1897
9. Yang HL, Liu T, Wang XM et al (2011) Diagnosis of bone metastases: a meta-analysis comparing 18FDG PET, CT, MRI and bone scintigraphy. Eur Radiol 21:2604–2617
10. Jambor I, Kuisma A, Ramadan S et al (2016) Prospective evaluation of planar bone scintigraphy, SPECT, SPECT/CT, 18F-NaF PET/CT and whole body 1.5T MRI, including DWI, for the detection of bone metastases in high risk breast and prostate cancer patients: SKELETA clinical trial. Acta Oncol 55:59–67
11. Takahara T, Yamashita T (2003) Diffusion weighted whole body imaging with background body signal suppression (DWIBS): technical improvement using free breathing, STIR and high resolution 3D display. Radiat Med 22:275–282
12. Padhani AR, Liu G, Mu-Koh D et al (2009) Diffusion-weighted magnetic resonance imaging as a cancer biomarker: consensus and recommendations. Neoplasia 11:102–125
13. Kosmin M, Padhani AR, Gogbashian A et al (2020) Comparison of whole-body MRI, CT, and bone scintigraphy for response evaluation of cancer therapeutics in metastatic breast cancer to bone. Radiology. 297:622–629
14. Padhani AR, Lecouvet FE, Tunariu N et al (2017) METastasis reporting and data system for prostate cancer: practical guidelines for acquisition, interpretation, and reporting of whole-body magnetic resonance imaging-based evaluations of multiorgan involvement in advanced prostate cancer [figure presente. Eur Urol 71:81–92
15. Johnson TRC, Krauß B, Sedlmair M et al (2007) Material differentiation by dual energy CT: initial experience. Eur Radiol 17:1510–1517
16. Fredenberg E (2018) Spectral and dual-energy X-ray imaging for medical applications. Nucl Instruments Methods Phys Res Sect A Accel Spectrometers, Detect Assoc Equip 878:74–87
17. Carmi R, Naveh G, Altman A (2005) Material separation with dual-layer CT. IEEE Nucl Sci Symp Conf Rec 4:1876–1878
18. McCollough CH, Leng S, Yu L, Fletcher JG (2015) Review: dual- and multi-energy CT. RSNA Radiology 276:637–653
19. Simons D, Kachelrieß M, Schlemmer HP (2014) Recent developments of dual-energy CT in oncology. Eur Radiol 24:930–939
20. Abdullayev N, Große Hokamp N, Lennartz S et al (2019) Improvements of diagnostic accuracy and visualization of vertebral metastasis using multi-level virtual non-calcium reconstructions from dual-layer spectral detector computed tomography. Eur Radiol 29:5941–5949
21. Andersen MB, Ebbesen D, Thygesen J et al (2020) Impact of spectral body imaging in patients suspected for occult cancer: a prospective study of 503 patients. Eur Radiol 30:5539–5550
22. Pesapane F, Downey K, Rotili A et al (2020) Imaging diagnosis of metastatic breast cancer. Insights Imaging 11:79
23. Heusner TA, Kuemmel S, Koeninger A et al (2010) Diagnostic value of diffusion-weighted magnetic resonance imaging (DWI) compared to FDG PET/CT for whole-body breast cancer staging. Eur J Nucl Med Mol Imaging 37:1077–1086
24. Fausto A, Bernini M, Giacomo LD et al (2018) Diagnostic value and safety of dynamic MRI of contralateral breast and axilla in subjects with tissue expander. J Plast Reconstr Aesthet Surg 71: 1282–1285
25. van Ommen F, de Jong HWAM, Dankbaar JW et al (2019) Dose of CT protocols acquired in clinical routine using a dual-layer detector CT scanner: a preliminary report. Eur J Radiol 112:65–71
26. van Ommen F, Bennink E, Vlassenbroek A et al (2018) Image quality of conventional images of dual-layer SPECTRAL CT: a phantom study. Med Phys 45:3031–3042
27. Fischer MA, Nanz D, Hany T et al (2011) Diagnostic accuracy of whole-body MRI/DWI image fusion for detection of malignant tumours: a comparison with PET/CT. Eur Radiol 21:246–255
28. Harris PA, Taylor R, Thielke R et al (2009) Research electronic data capture (REDCap)-A metadata-driven methodology and workflow process for providing translational research informatics support. J Biomed Inform 42:377–381
29. DeLong ER, DeLong DM, Clarke-Pearson DL (1988) Comparing the areas under two or more correlated receiver operating characteristic curves: a nonparametric approach. Biometrics 44:837–845
30. McNemar Q (1947) Note on the sampling error of the difference between correlated proportions or percentages. Psychometrika 12: 153–157
31. Zhang X, Zheng C, Yang Z et al (2018) Axillary sentinel lymph nodes in breast cancer: quantitative evaluation at dual-energy CT. Radiology 289:337–346
32. Volterrani L, Gentili F, Fausto A et al (2020) Dual-energy CT for locoregional staging of breast cancer: preliminary results. AJR Am J Roentgenol 214:707–714
33. Chae EJ, Song JW, Seo JB et al (2008) Clinical utility of dual-energy CT in the evaluation of solitary pulmonary nodules: Initial experience. Radiology 249:671–681
34. Schmid-Bindert G, Henzler T, Chu TQ et al (2012) Functional imaging of lung cancer using dual energy CT: how does iodine related attenuation correlate with standardized uptake value of 18FDG-PET-CT? Eur Radiol 22:93–103